Chapter 6

Probing Orbital Symmetry of Molecules Via Alignment-Dependent Ionization Probability and High-Order Harmonic Generation by Intense Lasers

Song-Feng Zhao*,†, Xiao-Xin Zhou* and C. D. Lin‡

*College of Physics and Electronic Engineering,
Northwest Normal University, Lanzhou, Gansu 730070, China
†Email: zhaosf@nwnu.edu.cn
‡J. R. Macdonald Laboratory, Physics Department,
Kansas State University, Manhattan, Kansas 66506-2604, USA

It is shown that measurement of alignment-dependent ionization probability and high-order harmonic generation (HHG) of molecules in an intense laser field can be used to probe the orbital symmetry of molecules. In this review, recent progress of molecular tunneling ionization (MO-ADK) model of Tong *et al.* [Phys. Rev. A 66, 033402 (2002)] is first reviewed. In particular, an efficient method to obtain wavefunctions of linear molecules in the asymptotic region was developed by solving the time-independent Schrödinger equation with B-spline functions, and molecular potential energy surfaces were constructed based on the density functional theory. The accurate wavefunctions are used to extract improved structure parameters in the MO-ADK model. The loss of accuracy of the MO-ADK model in the low intensity multiphoton ionization regime is also addressed by comparing with the molecular Perelomov–Popov–Terent'ev (MO-PPT) model, the single-active-electron time-dependent Schrödinger equation (SAE-TDSE) method, and the experimental data. Finally, how the orbital symmetry affects the HHG of molecules within the strong-field approximation (SFA) was reviewed.

1. Introduction

Probing molecular orbitals is one of the fundamental goals in physics and chemistry [1–5]. The conventional methods for studying the highest occupied molecular orbital (HOMO) are to use scanning tunneling microscopy (STM) [6, 7] and the angle-resolved photoelectron spectroscopy [8]. In 2004, based on the plane wave approximation, Itatani *et al.*, performed a complete tomographic reconstruction of the molecular *orbital wavefunction* of HOMO in N_2 from high harmonic spectra measured at various alignment angles [9]. Le *et al.*, examined the assumptions used in the tomographic procedure [10] and its underlying limitations. Since wavefunction in quantum mechanics is a complex function in general, it is a representation and not measurable. Thus the imaging of orbital wavefunction has to be taken with caution, and only within the confine of assumptions defined by the practitioners. The tomographic method has since been corrected by using scattering waves for the continuum states [11, 12], or by considering multielectron effects [13]. It has also been recently generalized to image the HOMO of asymmetric molecules [14]. The tomographic imaging is evidently based on the third recombination step of the three-step model of high-order harmonic generation (HHG) [15]. It is an indirect method and various approximations were made in the procedure. A more direct scheme, based on the first step (the ionization step), is to use the angle-dependent ionization rate (or probability) $P(\theta)$ of molecules, where θ is the angle between the molecular axis and the laser's polarization direction. Experimentally, the $P(\theta)$ has been obtained by ionizing a partially aligned ensemble of molecules [16–18, 20, 21]. Alternatively, the $P(\theta)$ can also be determined by measuring the molecular frame photoelectron angular distribution (MFPADs) [22–28] or by detecting the angular distribution of the emitted ionic fragments [29–34]. Theoretically, $P(\theta)$ can be calculated by solving the time-dependent Schrödinger equation (TDSE) of molecules, but often based on the single-active-electron (SAE) approximation [35–44] or by using the time-dependent density functional theory (TDDFT) [45–50]. Very recently, the time-dependent Hartree-Fock (TDHF) theory is also used to calculate the $P(\theta)$ of CO_2 [51]. Since these ab-initio calculations are rather time-consuming and still quite challenging for molecules, simpler theoretical models are quite desirable for interpreting experiments, such as the molecular Ammosov–Delone–Krainov model (MO-ADK) [52–55], the molecular strong-field approximation (MO-SFA) [56–60], the molecular Perelomov–Popov–Terent'ev (MO-PPT) model [61–63] and others [64–69].

Recall that the MO-ADK is a generalization of the atomic ADK model by Ammosov *et al.* [70] which was initially used to study the tunneling ionization of atoms. In the MO-ADK model [52], the static tunneling ionization rate is given analytically, and the rate depends on the molecular alignment angle, the

instantaneous electric field of the laser, the structure parameters C_{lm} of the outermost molecular orbital and its ionization potential. Once the structure parameters of a specific molecule are available, one can easily calculate the orientation-dependent ionization rate with the MO-ADK. Moreover, the ionization probabilities and signals can also be obtained readily by including the temporal profile and spatial distribution of a focused laser beam in order to compare with experiments. Thus it is essential to determine and tabulate accurate structure parameters for several occupied orbitals of molecules. These structure parameters can be extracted directly from the molecular orbital wavefunction in the asymptotic region. In Tong *et al.* [52], the molecular wavefunctions were calculated originally with the multiple-scattering method [71]. At the present time, molecular wavefunctions are commonly calculated from quantum chemistry codes, such as GAUSSIAN [72], GAMESS [73] and others [74, 75]. Using the Hartree-Fock (HF) approximation and the conventional Gaussian bases, molecular wavefunctions calculated from these packages have been used to extract structure parameters of HOMO for several linear molecules [39, 47, 48, 76] and for some nonlinear polyatomic molecules [55, 77]. With structure parameters determined from these two methods, the MO-ADK model fits reasonably well for most experimental $P(\theta)$, except for CO_2 [17]. In Zhao *et al.* [78], it was found that the large discrepancies of $P(\theta)$ between the MO-ADK and the experimental data [17] can be attributed partly to the inaccurate structure parameters of CO_2. To determine the accurate structure parameters of molecules, accurate wavefunction of the ionizing orbital in the asymptotic region is required. In [54, 78–81], an efficient method was proposed to fix the asymptotic tail of the molecular wavefunction by solving the time-independent Schrödinger equation with B-spline functions, where the molecular potential was constructed numerically based on the density-functional theory (DFT). Accurate structure parameters of the HOMO and some inner orbitals (i.e., HOMO-1 and HOMO-2) for many linear molecules have been determined and tabulated [54, 78–81]. Using these improved structure parameters in the MO-ADK model, the $P(\theta)$ of CO_2, C_2H_2, H_2^+ and H_2 were improved significantly by comparing with those from more elaborate calculations and experimental data in deed. This method has also been used to extract structure parameters from molecular wavefunction calculated by propagating the TDSE in imaginary time [39]. Recently, Madsen *et al.* [65] demonstrated that wavefunction of the HOMO with the correct exponential behavior can also be obtained directly by solving the HF equations with the X2DHF code for diatomic molecules. These accurate wavefunctions have been used to determine the structure parameters for the MO-ADK model [82] and the weak-field asymptotic theory (WFAT) [65]. For triatomic molecules such as CO_2, OCS and H_2O, the possibility of obtaining the correct asymptotic tail of the HOMO wavefunction using optimized Gaussian basis

sets from GAUSSIAN [72] or GAMESS [73] packages has been systematically studied [65, 66].

It is known that the alignment dependence of HHG is determined mostly by the orbital symmetry of molecules [9, 83]. In other words, it is possible to probe the HOMO orbital via the alignment-dependent HHG signals when contributions from inner orbitals (i.e., HOMO-1 and HOMO-2) are negligible. So far the alignment-dependent HHG has been studied theoretically by solving the TDSE of the simplest molecules such as H_2^+ [84–87] and HeH^{2+} [88, 89], or by performing the TDDFT calculations [90–93]. Since these two methods are rather time-consuming even for the single-molecule response of the HHG, most of the existing calculations for HHG from molecules were performed using the strong-field approximation (SFA) (to be called molecular Lewenstein) model [76, 94–101] which is a generalization of the atomic Lewenstein model [102]. In recent years, improvement on SFA has been proposed using the quantitative rescattering (QRS) theory [3, 103]. For large molecules, SFA can still be of interest in view of its simplicity and its reasonable accuracy.

The rest of this chapter is arranged as follows. In Sec. 2, the method of constructing one-electron potential of a linear molecule is summarized. This potential can be used to solve the time-independent Schrödinger equation with B-spline basis functions to fix the asymptotic tail of the molecular wavefunction. The basic equations of the MO-ADK, MO-PPT, MO-SFA and molecular Lewenstein models are then briefly reviewed. In Sec. 3, the improvement on the alignment dependence of ionization probability with the more accurate structure parameters is demonstrated. In this section, it is shown how to probe the orbital symmetry of molecules using the $P(\theta)$ and the alignment-dependent HHG signals by intense laser fields. A conclusion is given in Sec. 4.

2. Theoretical Methods

The theory part is separated into five subsections. First, it is shown on how to construct numerically one-electron potentials of linear molecules based on the DFT. Second, the method to improve the asymptotic tail of molecular wavefunction by solving the time-independent Schrödinger equation of linear molecules with B-spline functions and extract accurate structure parameters of molecules in the asymptotic region is given. Finally the basic equations of the MO-ADK, MO-PPT, MO-SFA and molecular Lewenstein models are reviewed, respectively.

2.1. *Construction of one-electron potentials of linear molecules*

The one-electron potentials are constructed numerically using the modified Leeuwen–Baerends (LBα) model [79, 80, 104, 105] where the electrostatic and exchange-correlation terms are included.

For linear molecules, based on the single-center expansion, the one-electron potential can be expressed as

$$V(r,\theta_e) = \sum_{l=0}^{l_{\max}} v_l(r) P_l(\cos\theta_e). \tag{1}$$

Here, $v_l(r)$ is the radial component of the molecular potential and $P_l(\cos\theta_e)$ is the Legendre polynomial, θ_e is the angular coordinate of the active electron in the molecular frame. The radial potential is given by

$$v_l(r) = v_l^{nuc}(r) + v_l^{el}(r) + v_l^{xc}(r), \tag{2}$$

where the first two terms represent the electrostatic potential and the last term is the exchange-correlation interaction.

The electron-nucleus interaction $v_l^{nuc}(r)$ can be written as

$$v_l^{nuc}(r) = \sum_{i=1}^{N_a} v_l^i(r), \tag{3}$$

where i sums over all the N_a atoms in the molecule. By assuming the linear molecule is aligned along the z-axis, $v_l^i(r)$ is given by

$$v_l^i(r) = \begin{cases} -\left(\dfrac{r_<^i}{r_>^i}\right)^l \dfrac{Z_c^i}{r_>^i} & \text{if } z_i > 0 \\ -(-1)^l \left(\dfrac{r_<^i}{r_>^i}\right)^l \dfrac{Z_c^i}{r_>^i} & \text{if } z_i < 0. \end{cases} \tag{4}$$

Here, $r_<^i = \min(r, |z_i|)$ and $r_>^i = \max(r, |z_i|)$. Z_c^i and z_i are the nuclear charge and the z coordinate of the ith atom, respectively.

The partial Hartree potential $v_l^{el}(r)$ is written as

$$v_l^{el}(r) = \frac{4\pi}{2l+1} \int_0^\infty a_l(r') r'^2 \frac{r_<^l}{r_>^{l+1}} dr' \tag{5}$$

with $r_< = \min(r, r')$ and $r_> = \max(r, r')$. Here $a_l(r')$ is determined by

$$a_l(r') = \frac{2l+1}{2} \int_{-1}^{1} \rho(r', \theta_e') P_l(\cos\theta_e') d(\cos\theta_e') \tag{6}$$

where $\rho(r', \theta_e')$ is the total electron density and

$$\rho(r', \theta_e') = \sum_{i=1}^{N_e} \frac{1}{2\pi} \int_0^{2\pi} \left|\Psi_i(r', \theta_e', \varphi_e')\right|^2 d\varphi_e' \tag{7}$$

with i runs over all the N_e electrons. The wavefunction of each molecular orbital can be calculated from quantum chemistry codes such as GAUSSIAN [72] and GAMESS [73].

In the LBα model, the partial exchange-correlation potential can be expressed as

$$v_l^{xc}(r) = \frac{2l+1}{2}\int_{-1}^{1} V_{xc,\sigma}^{LB\alpha}(r,\theta_e)\,P_l(\cos\theta_e)d(\cos\theta_e) \tag{8}$$

where

$$V_{xc,\sigma}^{LB\alpha}(r,\theta_e) = \alpha V_{x,\sigma}^{LDA}(r,\theta_e) + V_{c,\sigma}^{LDA}(r,\theta_e) - \frac{\beta\chi_\sigma^2(r,\theta_e)\rho_\sigma^{1/3}(r,\theta_e)}{1+3\beta\chi_\sigma(r,\theta_e)\sinh^{-1}[\chi_\sigma(r,\theta_e)]} \tag{9}$$

with $\chi_\sigma(r,\theta_e) = |\nabla\rho_\sigma(r,\theta_e)|\rho_\sigma^{-4/3}(r,\theta_e)$ and $\rho_\sigma(r,\theta_e)$ is spin density. Here α and β are two empirical parameters. $V_{x,\sigma}^{LDA}(r,\theta_e)$ is the local density approximation (LDA) exchange potential

$$V_{x,\sigma}^{LDA}(r,\theta_e) = -\left[\frac{6}{\pi}\rho_\sigma(r,\theta_e)\right]^{1/3}. \tag{10}$$

In the present LBα calculations, the LDA correlation potential $V_{c,\sigma}^{LDA}(r,\theta_e)$ is calculated by using the Perdew–Wang representation for the correlation functionals [106]

$$V_{c,\sigma}^{LDA}(r,\theta_e) = \varepsilon_c(r_s,\zeta) - \frac{r_s}{3}\frac{\partial\varepsilon_c(r_s,\zeta)}{\partial r_s} - (\zeta - \mathrm{sgn}\,\sigma)\frac{\partial\varepsilon_c(r_s,\zeta)}{\partial\zeta}, \tag{11}$$

where r_s and ζ are the density parameter and the relative spin polarization, respectively, and $\varepsilon_c(r_s,\zeta)$ is the correlation energy. Note that sgnσ is 1 for $\sigma = \uparrow$ and -1 for $\sigma = \downarrow$.

2.2. *Calculation of molecular wavefunction with correct asymptotic tail by solving the time-independent Schrödinger equation*

Using the molecular potentials constructed in the previous subsection, the molecular wavefunction with the correct asymptotic behavior can be obtained by solving the following time-independent Schrödinger equation for linear molecules [54, 78–81]

$$H_{el}\Psi_n^{(m)}(\vec{r}) \equiv \left[-\frac{1}{2}\nabla^2 + V(r,\theta_e)\right]\Psi_n^{(m)}(\vec{r}) = E_n^{(m)}\Psi_n^{(m)}(\vec{r}), \tag{12}$$

where m is z component of the electronic orbital momentum and n is the orbital index. Because of the cylindrical symmetry, the wavefunction $\Psi_n^{(m)}(\vec{r})$ can be written as

$$\Psi_n^{(m)}(\vec{r}) = \frac{1}{\sqrt{2\pi}} e^{im\chi_e} \psi(r, \xi). \tag{13}$$

Here, $\xi = \cos\theta_e$ and χ_e is the angular coordinate of the active electron in the molecular frame. The wavefunction $\psi(r, \xi)$ can be expanded by B-spline functions as [80, 107]

$$\psi(r, \xi) = \sum_{i=1}^{N_r} \sum_{j=1}^{N_\xi} C_{ij} B_i(r)(1 - \xi^2)^{|m|/2} B_j(\xi), \tag{14}$$

where $B_i(r)$ and $B_j(\xi)$ are radial and angular B-spline functions, respectively. By substituting Eqs. (1), (13), and (14) into Eq. (12) and projecting onto the basis set $B_{i'}(r)(1 - \xi^2)^{|m|/2} B_{j'}(\xi)$, we obtain the following matrix equation

$$HC = ESC, \tag{15}$$

with

$$\begin{aligned} H_{i'j',ij} = &\int_0^{r_{\max}} \int_{-1}^{1} B_{i'}(r)(1 - \xi^2)^{|m|/2} B_{j'}(\xi) H_{el} \\ &\times B_i(r)(1 - \xi^2)^{|m|/2} B_j(\xi) r^2 dr d\xi, \end{aligned} \tag{16}$$

and

$$\begin{aligned} S_{i'j',ij} = &\int_0^{r_{\max}} B_{i'}(r) B_i(r) r^2 dr \\ &\times \int_{-1}^{1} B_{j'}(\xi)(1 - \xi^2)^{|m|} B_j(\xi) d\xi, \end{aligned} \tag{17}$$

where E and C are energy matrix and coefficient matrix, respectively. The eigenfunctions and eigenvalues for a given m can be obtained by diagonalizing Eq. (15).

For linear molecules, based on the single-center expansion, wavefunctions can also be expanded as

$$\Psi_n^{(m)}(\vec{r}) = \sum_l F_{lm}(r) Y_{lm}(\theta_e, \chi_e), \tag{18}$$

where $Y_{lm}(\theta_e, \chi_e)$ is the spherical harmonic functions. The radial wavefunction can be calculated by

$$F_{lm}(r) = \int \Psi_n^{(m)}(\vec{r}) Y_{lm}^*(\theta_e, \chi_e) \sin\theta_e d\theta_e d\chi_e. \tag{19}$$

Then accurate structure parameters C_{lm} can be determined by matching these radial functions to the form

$$F_{lm}(r) = C_{lm} r^{(Z_c/\kappa)-1} e^{-\kappa r} \tag{20}$$

where Z_c is the asymptotic charge, $\kappa = \sqrt{2I_p}$, and I_p is the ionization energy.

In the molecular frame, the angular distribution of the asymptotic electron density for the active electron can be written as

$$\rho_1(\theta_e, \chi_e) = \int_{r_1}^{\infty} \left|\Psi_n^{(m)}(r, \theta_e, \chi_e)\right|^2 r^2 dr \tag{21}$$

r_1 is the starting point of the fitting range. The θ_e-dependent electron density is given by

$$\rho(\theta_e) = \frac{1}{2\pi} \int_0^{2\pi} \rho_1(\theta_e, \chi_e) d\chi_e. \tag{22}$$

2.3. *The MO-ADK and MO-PPT models*

According to the MO-ADK model [52, 55, 77], the cycle-averaged ionization rate is given by

$$w_{MO-ADK}(F, \vec{R}) = \left[\frac{3F}{\pi k^3}\right]^{1/2} \sum_{m'} \frac{B^2(m')}{2^{|m'|}|m'|!} \frac{1}{\kappa^{2Z_c/\kappa-1}} \left(\frac{2\kappa^3}{F}\right)^{2Z_c/\kappa-|m'|-1} e^{-2\kappa^3/3F}, \tag{23}$$

where F is the peak field strength and $\vec{R} \equiv (\phi, \theta, \chi)$ is the Euler angles of the molecular frame with respect to the laboratory frame. Note that θ is the angle between the Z and z axes, ϕ and χ denote rotations around the Z axis and the z axis, respectively. For linear molecules, $B(m')$ can be expressed as

$$B(m') = \sum_l C_{lm} D^l_{m',m}(\vec{R}) Q(l, m'). \tag{24}$$

For nonlinear molecules, m is no longer a good quantum number and thus $B(m')$ is written as

$$B(m') = \sum_{lm} C_{lm} D^l_{m',m}(\vec{R}) Q(l, m'), \tag{25}$$

with

$$Q(l,m') = (-1)^{(m'+|m'|)/2}\sqrt{\frac{(2l+1)(l+|m'|)!}{2(l-|m'|)!}}, \tag{26}$$

and $D^l_{m',m}(\vec{R})$ is the Wigner rotation matrix

$$D^l_{m',m}(\vec{R}) = e^{-im'\phi}d^l_{m',m}(\theta)e^{-im\chi}. \tag{27}$$

Based on the MO-PPT model [61, 63], the cycle-averaged ionization rate can be calculated analytically by

$$w_{MO-PPT}(F,\omega,\vec{R}) = \left(\frac{3F}{\pi k^3}\right)^{1/2}\sum_{m'}\frac{B^2(m')}{2^{|m'|}\,|m'|!}\frac{A_{m'}(\omega,\gamma)}{\kappa^{2Z_c/\kappa-1}}(1+\gamma^2)^{|m'|/2+3/4} \times\left(\frac{2\kappa^3}{F}\right)^{2Z_c/\kappa-|m'|-1} e^{\left[-(2\kappa^3/3F)g(\gamma)\right]}, \tag{28}$$

where γ is the Keldysh parameter and ω is the angular frequency of the laser pulse. The coefficients $A_{m'}(\omega,\gamma)$ can be found in Refs. [62, 108, 109]. $g(\gamma)$ is given by

$$g(\gamma) = \frac{3}{2\gamma}\left[(1+\frac{1}{2\gamma^2})\sinh^{-1}\gamma - \frac{\sqrt{1+\gamma^2}}{2\gamma}\right]. \tag{29}$$

With the cycle-averaged ionization rates of molecules, one can calculate the total ionization probability by a laser pulse by

$$P(I,\vec{R}) = 1-\exp(-\int_{-\infty}^{+\infty} w_m(F,\vec{R})dt), \tag{30}$$

where m stands for the MO-ADK or the MO-PPT model.

To compare with experimental data, the ionization signal of molecules has to be calculated by

$$S(\vec{R}) \propto \int P(I,\vec{R})2\pi r dr dz = \int_0^{I_0} P(I,\vec{R})\left[-\frac{\partial V}{\partial I}\right]dI \tag{31}$$

Here, I_0 is the peak intensity at the focal point and the volume element takes the form $-dV/dI \propto (2I+I_0)(I_0-I)^{1/2}I^{-5/2}$. The spatial component of the electric field is assumed to be a Gaussian beam in our simulations.

2.4. *Calculation of the orientation-dependent ionization probability of molecules with the MO-SFA model*

Based on the MO-SFA [80, 103], the total ionization probability of molecules by a laser pulse can be written as

$$P(\vec{R}) = \int \left| f(\vec{p}, \vec{R}) \right|^2 d^3\vec{p}, \tag{32}$$

with

$$f(\vec{p}, \vec{R}) = i \int_{-\infty}^{+\infty} \left\langle \vec{p} + \vec{A}(t) \middle| \vec{r} \cdot \vec{E}(t) | \Phi_0(\vec{r}) \right\rangle e^{-iS(\vec{p},t)} dt, \tag{33}$$

where $\vec{p}$ is the momentum of the emitted electron, $\vec{E}(t)$ and $\vec{A}(t)$ are the electric field and the vector potential, respectively. The action $S(\vec{p}, t)$ is given by

$$S(\vec{p}, t) = \int_t^{\infty} dt' \left\{ \frac{\left[\vec{p} + \vec{A}(t')\right]^2}{2} + I_p \right\}. \tag{34}$$

In Eq. (33), the ground-state wavefunction $\Phi_0(\vec{r})$ can be obtained from GAUSSIAN [72] or GAMESS [73] and the continuum state is approximated by a Volkov state.

2.5. *The molecular Lewenstein model for HHG from molecules*

In earlier work [94, 95], the Lewenstein model [102] was first generalized to diatomic molecules. It is then modified by others [76, 96–101]. According to the SFA, the parallel component of the induced dipole moment of a molecule driven by a linearly polarized laser field can be written as [110]

$$\begin{aligned} x(t) = i \int_0^{\infty} d\tau \left(\frac{\pi}{\varepsilon + i\tau/2} \right)^{3/2} \\ \times [\sin\theta \cos\chi d_x^*(t) + \sin\theta \sin\chi d_y^*(t) + \cos\theta d_z^*(t)] \\ \times [\sin\theta \cos\chi d_x(t-\tau) + \sin\theta \sin\chi d_y(t-\tau) + \cos\theta d_z(t-\tau)] \\ \times E(t-\tau) \exp[-iS_{st}(t,\tau)] a^*(t) a(t-\tau) + c.c., \end{aligned} \tag{35}$$

with ε being a positive regularization constant. Here, $d_x(t)$, $d_y(t)$, and $d_z(t)$ are the x, y, and z components of the transition dipole moment between the ground state and the continuum state. The quasiclassical action at the stationary points for the

electron propagating in the laser field is given by

$$S_{st}(t,\tau) = \int_{t-\tau}^{t} \left(\frac{\left[p_{st}(t,\tau) + A(t')\right]^2}{2} + I_p \right) dt', \tag{36}$$

where the canonical momentum at the stationary points is expressed as

$$p_{st}(t,\tau) = -\frac{1}{\tau} \int_{t-\tau}^{t} dt' A(t'). \tag{37}$$

In Eq. (35), $a(t)$ is introduced to account for the ground-state depletion and

$$a(t) = \exp\left[-\frac{1}{2} \int_{-\infty}^{t} w(t') dt' \right], \tag{38}$$

with the ionization rate $w(t')$ obtained from the MO-ADK model [52, 54, 55]. Again the ground state wavefunction of the molecule is calculated using the standard quantum chemistry program like GAUSSIAN [72] and the continuum state is described approximately with a plane wave. We note that Eq. (35) can be reduced to Eq. (4) in Ref. [95] if a linear molecule aligned along the z axis is exposed to a laser field, linearly polarized on the y-z plane.

3. Results and Discussions

3.1. *The one-electron potentials for* Cl_2

The model potentials of H_2 and N_2 were proposed in Refs. [41, 111], respectively. However, most of the effective potentials are calculated numerically based on the DFT [38, 39, 45–50, 54, 78–80, 90–93]. The one-electron potentials for linear molecules are created numerically following the procedure described in Sec. 2.1. Figure 1 shows partial wave expansions ($v_l^{nuc}(r)$, $v_l^{el}(r)$, $v_l^{xc}(r)$, and $v_l(r)$) of the effective potential $V(r,\theta_e)$ (see Eqs. (1) and (2)) for Cl_2.

3.2. *Extracting structure parameters for several highly occupied orbitals of linear molecules*

Once the wavefunctions with the correct asymptotic tail and the corresponding orbital binding energies of linear molecules are obtained by solving Eq. (12), accurate structure parameters can be extracted from these molecular wavefunctions in the asymptotic region. It has been confirmed that the calculated LBα orbital binding energies are in good agreement with the experimental data [45, 46, 50, 79, 80]. Figure 2 shows the radial wavefunctions of H_2^+ and CO_2 for the first three partial waves and compared to those obtained directly from the GAUSSIAN. In the small-r

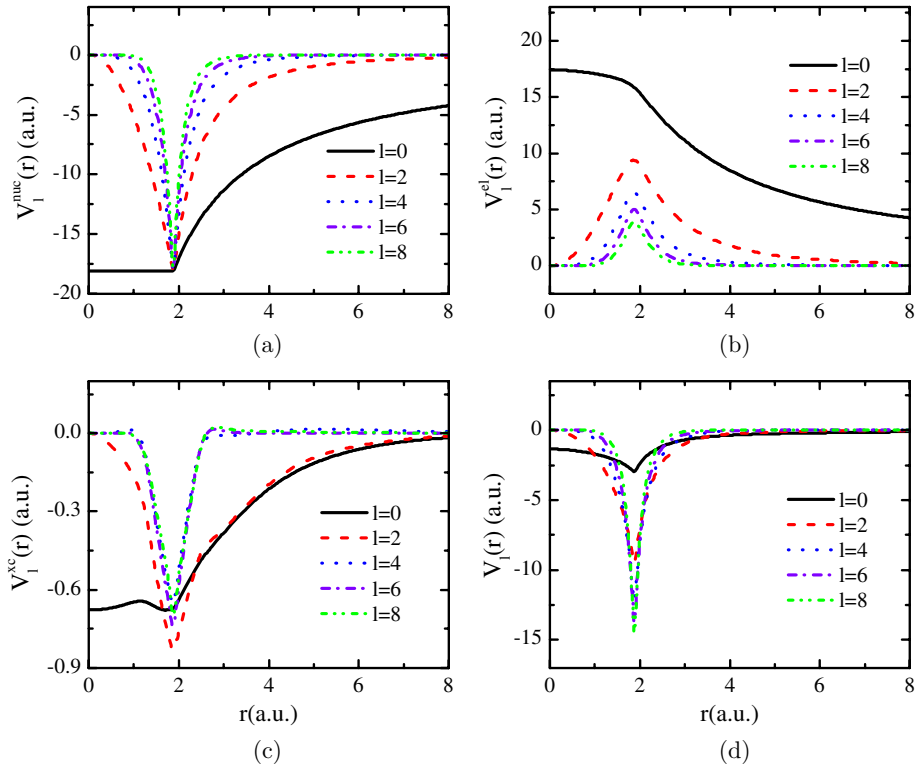

Fig. 1. (Color online) (a) Partial wave decomposition of the electron-nucleus potential; (b) the same for electron-electron repulsion potential; (c) for the exchange-correlation potential; (d) the total potential for each partial wave. We take $l_{max} = 80$ for Cl_2, but only low $l = 0, 2, 4, 6, 8$ terms are shown for clarity. Adapted from [80]. © (2013) by Taylor & Francis.

region, the present radial function agrees quite well with those from the GAUSSIAN for each partial wave. In the large-r region, one can see clearly the present calculated radial function displays the exponential decay form of Eq. (20). However, those from the GAUSSIAN exhibit oscillations and drop much faster like a Gaussian function. Note that conventional Gaussian bases are used in our present GAUSSIAN calculations. To determine the structure parameters of molecules, i.e., comparison of the asymptotic behavior of the calculated radial function to the correct asymptotic behavior [see Eq. (20)], the method proposed in Ref. [57] was followed. In Fig. 3, the structure parameters of H_2^+ at the equilibrium distance are obtained by fitting the calculated radial function to the correct one. The structure parameters C_{00}, C_{20} and C_{40} are 4.52, 0.62, 0.03, respectively. Using this method, we determined and tabulated structure parameters of the HOMO and of some inner orbitals for 37 linear molecules [54, 78–81].

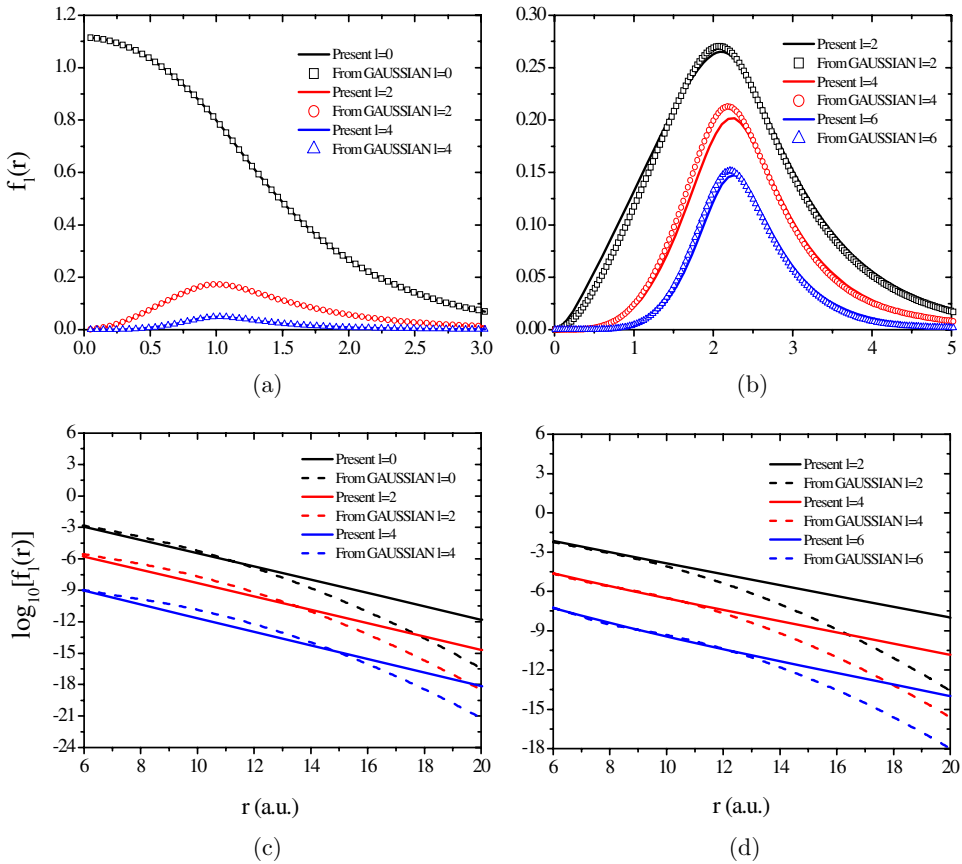

Fig. 2. (Color online) Partial wave radial function in the small-r region: (a) H_2^+; (b) CO_2 and in the large-r region: (c) H_2^+; (d) CO_2. For clarity, in (c) and (d), the radial functions for the last two partial waves are divided by 10^2 and 10^4, respectively. Figs. 2(b) and (d) are adapted from [78]. © (2009) by the American Physical Society.

3.3. *Comparison of alignment dependent ionization probabilities between the MO-ADK model and other more elaborate calculations*

Using the improved coefficients tabulated in Refs. [39, 54, 78–82], one can now calculate alignment dependent ionization probabilities for several selected molecules that have also been carried out by other theoretical methods. The comparison of these results is shown in Fig. 4. For simplicity, all the probabilities are normalized to 1.0 at the peak. For H_2^+ and H_2, one can see the MO-ADK results using the improved C_{lm} exhibit stronger angular dependence than the old ones (see Figs. 4(a) and 4(b)). The present MO-ADK results are in good agreement with those from TDSE [37, 40] for H_2^+ and with those from TDDFT [47] for H_2, respectively.

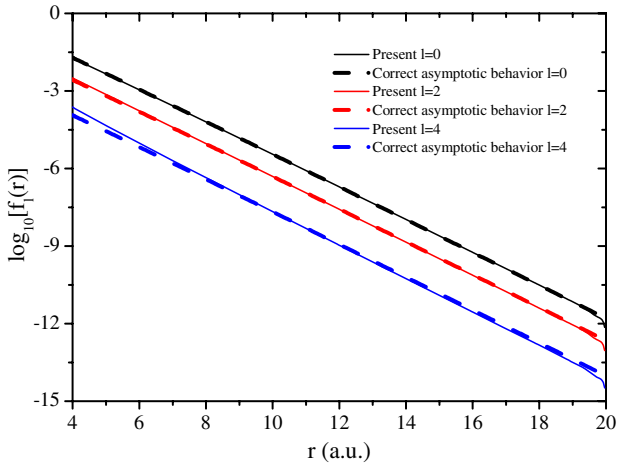

Fig. 3. (Color online) Comparison of the asymptotic behavior of the present calculated radial wavefunction (solid) to the correct asymptotic behavior (dashed) for H_2^+.

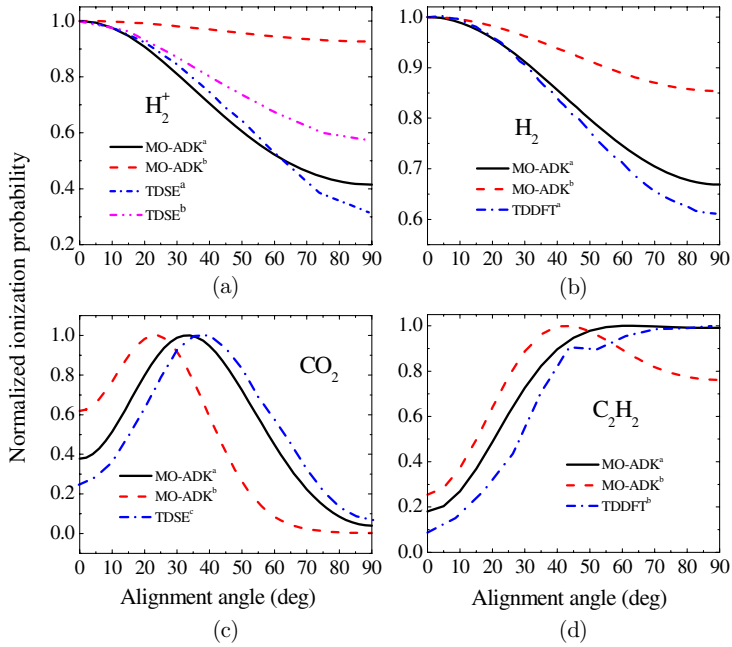

Fig. 4. (Color online) Normalized alignment-dependent ionization probability. (a) H_2^+ at 5×10^{14} W/cm^2; (b) H_2 at 1×10^{14} W/cm^2; (c) CO_2 at 1.1×10^{14} W/cm^2; (d) C_2H_2 at 5×10^{13} W/cm^2. MO-ADK^a denotes MO-ADK results using the present improved C_{lm} coefficients [54, 78], MO-ADK^b stands for MO-ADK results using the original C_{lm} coefficients determined from the multiple scattering theory [52, 76], TDSE^a from Kamta *et al.* [40], TDSE^b from Kjeldsen *et al.* [37], TDSE^c from Petretti *et al.* [35], TDDFT^a from Chu [47], and TDDFT^b from Otobe *et al.* [49]. Fig. 4(a) is adapted from [54].

For CO_2, the present MO-ADK peaks at 35° instead of 24° from the MO-ADK using the old coefficients. The improved MO-ADK result is much closer to the peak at 40° predicted by TDSE [35]. For C_2H_2, the older MO-ADK result has a peak at 45° and gives a minimum at 90°, while the TDDFT result [49] shows a peak at 90°. The new MO-ADK result agrees well with that from the TDDFT.

3.4. *Comparison with experiments*

It has been confirmed that the MO-ADK results using old coefficients agree reasonably well with the experimental data for N_2 and O_2 [16, 17, 31, 54]. For CO_2, The larger discrepancies of alignment-dependent ionization probabilities between the older MO-ADK results and the experimental data were found in Ref. [17]. The discrepancy brought out by the experiment [17] attracted a number of more accurate theoretical calculations such as the TDSE [39, 112], TDHF [51], and TDDFT [45]. For H_2, the original MO-ADK underestimates the experimental ratio of ionization rate for molecules aligned parallel vs. perpendicular with respect to the molecular axis [22, 31], while the present MO-ADK overestimates the experimental ratio [54]. The correct ratios have been obtained by solving the TDSE with a model potential at different laser intensities [41]. In Fig. 5(a), the normalized ionization probabilities of CO_2 from several theoretical methods with the experimental data for laser intensity $I = 1.1 \times 10^{14}\,\mathrm{W/cm^2}$ are compared. One can see the peak positions determined from the TDSE and the TDDFT are much closer to the experimental one than the MO-ADK result. However, so far all the theoretical results available fail to predict the narrow ionization distribution reported in the experiment. For laser intensity $I = 0.3 \times 10^{14}\,\mathrm{W/cm^2}$, the experimental data show a very broad angular distribution, consistent with all the theoretical results (see Fig. 5(b)). The reasonable agreement of the peak positions between these theoretical calculations and the experimental measurement can be observed in Fig. 5(b).

3.5. *Alignment dependence of ionization rates from HOMO, HOMO-1, and HOMO-2 orbitals*

In recent years, strong-field phenomena involving inner orbitals of molecules have been studied widely [23, 27, 28, 31, 35, 36, 45, 54, 79, 80, 113–122]. Since tunneling ionization is the first fundamental step to all rescattering processes including the HHG, it is important to investigate at what orientation (or alignment) angles the contributions from inner orbitals have to be considered by comparing the $P(\theta)$ of the HOMO with those from inner orbitals of molecules. Clearly the $P(\theta)$ of inner orbitals can also be calculated easily by the MO-ADK model using the corresponding experimental ionization potentials and structure parameters tabulated in Refs. [54, 79, 80]. Figure 6 shows the orientation-dependent ionization rates from the

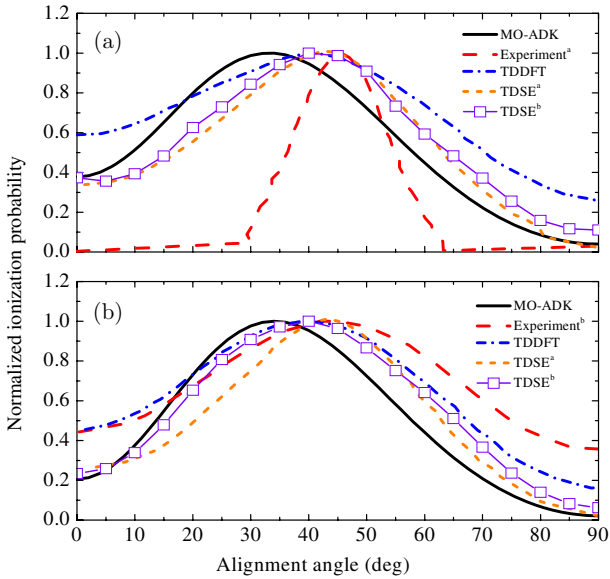

Fig. 5. (Color online) Normalized alignment-dependent ionization probabilities of CO_2. (a) Laser intensity is 1.1×10^{14} W/cm^2; (b) Laser intensity is 0.3×10^{14} W/cm^2. Note that 0.5×10^{14} W/cm^2 and 0.56×10^{14} W/cm^2 were used in Refs. [39, 45], respectively. TDDFT from Ref. [45], TDSE^a from Ref. [39], TDSE^b from Ref. [112], Experiment^a from Ref. [17], and Experiment^b from Ref. [18].

HOMO, HOMO-1, and HOMO-2 for N_2, CO_2, and Cl_2 and those from HOMO and HOMO-1 for the HBr molecule, respectively. Note that the angular dependence of ionization rates, $P(\theta)$, reflects vividly the shape of molecular orbitals. For the $P(\theta)$, a σ_g (or σ_u) orbital tends to have a peak at 0° and a minimum at 90°, a π orbital has the peak at 90° and minimum at 0° and 180°, a π_g orbital gives the peak near 45° and minimum at 0° and 90°, and a π_u orbital demonstrates a peak at 90° and a minimum at 0°. In Figs. 6(a) and 6(b), one can see that the contributions of ionization from HOMO-1 near 90° for N_2 and from HOMO-2 near 0° for CO_2 should be taken into account. Indeed, the contributions from the HOMO-1 (HOMO-2) to the HHG of N_2 (CO_2) have been reported widely [115–122]. For Cl_2, the contributions of ionization from the HOMO-1 near 90° and from the HOMO-2 near 0° are comparable to those from the HOMO (see Fig. 6(c)). For HBr, the ionization rates of the HOMO-1 are much higher than those of the HOMO near 180°. The significant contributions of ionization from the HOMO-1 near 0° and 180° can be seen in Fig. 6(d).

3.6. *Probing the shape of the ionizing molecular orbitals with the orientation-dependent ionization rates*

It has been confirmed that the orientation dependent ionization rates can reflect vividly the orbital symmetry of molecules [16, 17, 22, 28, 40, 54, 55]. In Fig. 7, the orientation dependent ionization rate $P(\theta)$ with the angle-dependent asymptotic

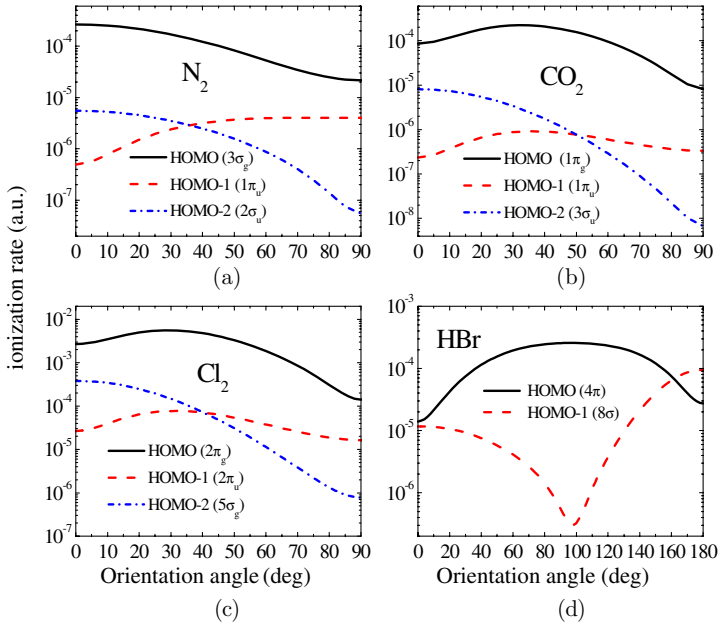

Fig. 6. (Color online) Orientation-dependent ionization rates of HOMO, HOMO-1, and HOMO-2 for N_2, CO_2, and Cl_2 and of HOMO and HOMO-1 for HBr. (a) N_2 at laser intensity of 1.5×10^{14} W/cm^2; (b) CO_2 at 1.1×10^{14} W/cm^2; (c) Cl_2 at 6.9×10^{13} W/cm^2; (d) HBr at 7.2×10^{13} W/cm^2. Figs. 6(a) and (b) are adapted from [54]. © (2010) by the American Physical Society. Figs. 6(c) and (d) are adapted from [80]. © (2013) by Taylor & Francis.

electron density $\rho(\theta_e)$ of the HOMO orbital for N_2, O_2, CO, and HBr are compared, respectively. Here, the MO-ADK model is used to calculate the $P(\theta)$ of these four linear molecules. One can see that the $P(\theta)$ follows well the shape of $\rho(\theta_e)$, as shown in Fig. 7. Note that the structure parameters C_{lm} of CO are taken from Ref. [80]. For the planar H_2O molecule, the molecule lies on the y-z plane, with the O atom along the z axis. The isocontour plot of the HOMO wavefunction is shown in Fig. 8(c). Clearly the HOMO orbital contains a nodal plane (i.e., y-z plane). The angular dependence of electron density is quite similar to that of ionization rate (see Figs. 8(a) and 8(b)). By averaging the electron density $\rho_1(\theta_e, \chi_e)$ and ionization rate $P(\theta, \chi)$ over χ_e or χ, the θ dependent ionization rate agrees very well with the electron density, as shown in Fig. 8(d). Thus it is possible to probe directly the electron density of the molecular orbital from which the electron is tunnel ionized using the corresponding alignment-dependent ionization rates when the ionization contributions from other occupied orbitals can be ignored.

3.7. *Examination of the validity of the MO-ADK and MO-PPT models*

Next the MO-ADK and MO-PPT models are examined by comparing them to the SAE-TDSE calculations and the experimental results. It has been confirmed that

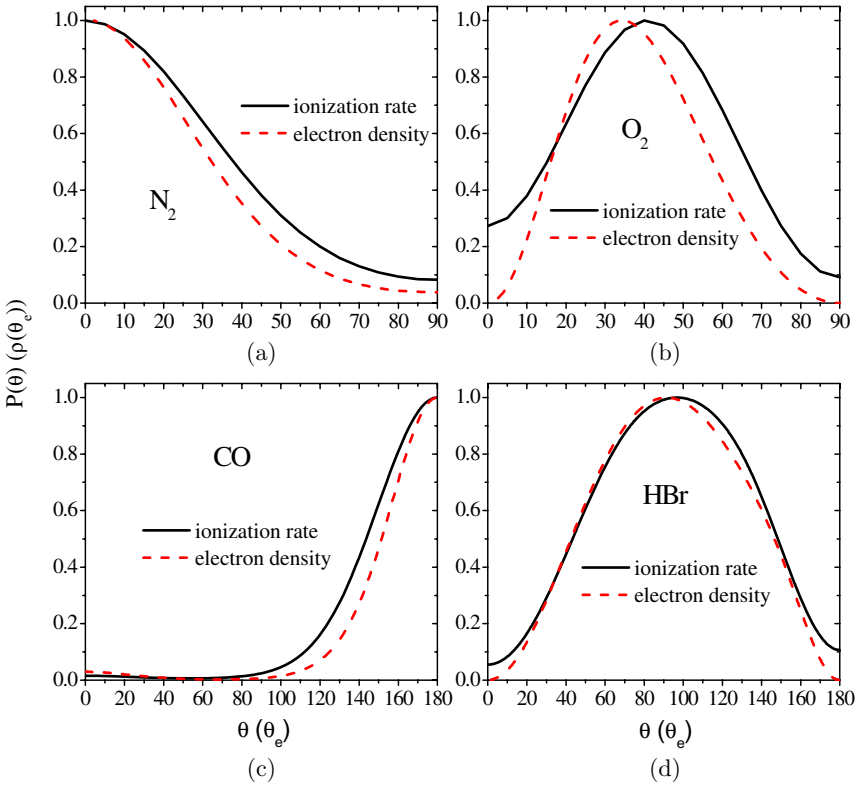

Fig. 7. (Color online) Comparison of the orientation-dependent ionization rate (solid line) to the angular distribution of asymptotic electron density (dashed line). The ionization rates are obtained from the MO-ADK model. (a) N_2 at laser intensity of 1.0×10^{14} W/cm^2; (b) O_2 at 1.0×10^{14} W/cm^2; (c) CO at 1.9×10^{14} W/cm^2; (d) HBr at 7.2×10^{13} W/cm^2.

the MO-ADK model works well in the tunneling ionization regime. This model has also been empirically modified to study the ionization of the H_2^+ molecule in the over-the-barrier ionization (TBI) regime [123]. However, the MO-ADK model is not valid in the multiphoton ionization regime [52, 62, 63]. Figure 9 compares the present calculated ionization probabilities of H_2 from the MO-ADK and MO-PPT models with those SAE-TDSE results using the Hartree-Fock functionals [43]. All the ionization probabilities from the MO-ADK and MO-PPT models are normalized to those of the SAE-TDSE at the saturation laser intensity of 2.29×10^{14} W/cm^2. One can see that the MO-ADK fits quite well the SAE-TDSE in the tunneling ionization region (i.e., $\gamma < 1$), while it underestimates remarkably the ionization probabilities in the multiphoton ionization regime indeed (i.e., $\gamma > 1$). The MO-PPT agrees very well with the SAE-TDSE in the whole range covering from the multiphoton to tunneling ionization regimes. In Fig. 10, ionization signals of NO, Cl_2, N_2 and O_2 obtained from the MO-ADK and MO-PPT models with the experimental data

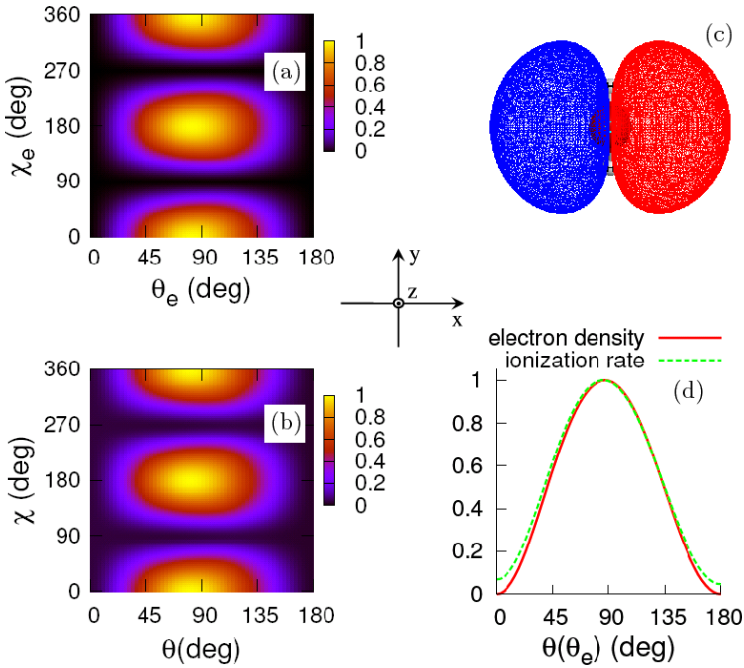

Fig. 8. (Color online) (a) Angular distribution of the normalized asymptotic electron density for H_2O. (b) Normalized alignment-dependent ionization rate of H_2O at laser intensity of 8×10^{13} W/cm^2. (c) The isocontour plot of the HOMO wavefunction for H_2O. The sign of the HOMO wavefunction is indicated by different colors, i.e., red denotes positive sign and blue stands for negative sign. (d) Comparison of the normalized χ_e or χ averaged electron density and ionization rate for H_2O. The x, y, z axes of the molecular frame are also shown. Adapted from [55]. © (2011) by IOP Publishing.

[52, 61, 124] are compared. Clearly the MO-PPT fits well with the experimental results, while the MO-ADK deviates seriously from the experimental data in the multiphoton ionization region.

3.8. *Probing the molecular orbital with the alignment-dependent HHG signals*

Finally, the possibility for probing the molecular orbital using the alignment-dependent HHG signals from molecules fixed in space is investigated. Here, HHG signals at several alignment angles from the molecular Lewenstein model are shown. In Fig. 11(a), the angular dependence of the yields of the 35th, 39th, and 43rd harmonics with angle-dependent asymptotic electron density for N_2 are compared. The HHG yield of each of the $(2n + 1)$-th harmonic is obtained by integrating over the intensity within the energy between the $2n$-th and $(2n + 2)$-th order. For simplicity, all the HHG yields and electron densities in Fig. 11 are normalized to 1.0 at the peak. For O_2, direct comparison of the alignment-dependent yields of

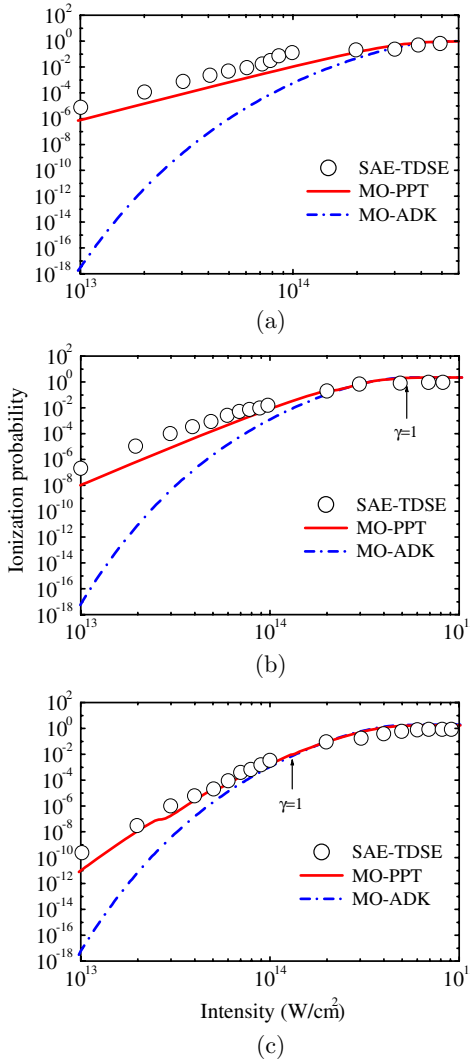

Fig. 9. (Color online) Ionization probabilities of the H_2 molecule as a function of laser peak intensity at central wavelengths of (a) 266 nm; (b) 400 nm; and (c) 800 nm. The laser field is a cosine square pulse with 36 cycles, 24 cycles and 12 cycles for 266 nm, 400 nm and 800 nm, respectively. SAE-TDSE from Ref. [43]. Adapted from [63]. © (2014) by Elsevier.

the 23rd, 27th, and 31st to the electron density is also shown in Fig. 11(b). In the present simulations, a Gaussian pulse with laser intensity of 3×10^{14} W/cm^2 for N_2 and 2×10^{14} W/cm^2 for O_2 was used, respectively. The central wavelength and the pulse duration are chosen to be 800 nm and 30 fs, respectively. In Figs. 11(a) and 11(b), the angular dependence among the different harmonics does not change much for N_2 and O_2, respectively. It is emphasized that the alignment dependence

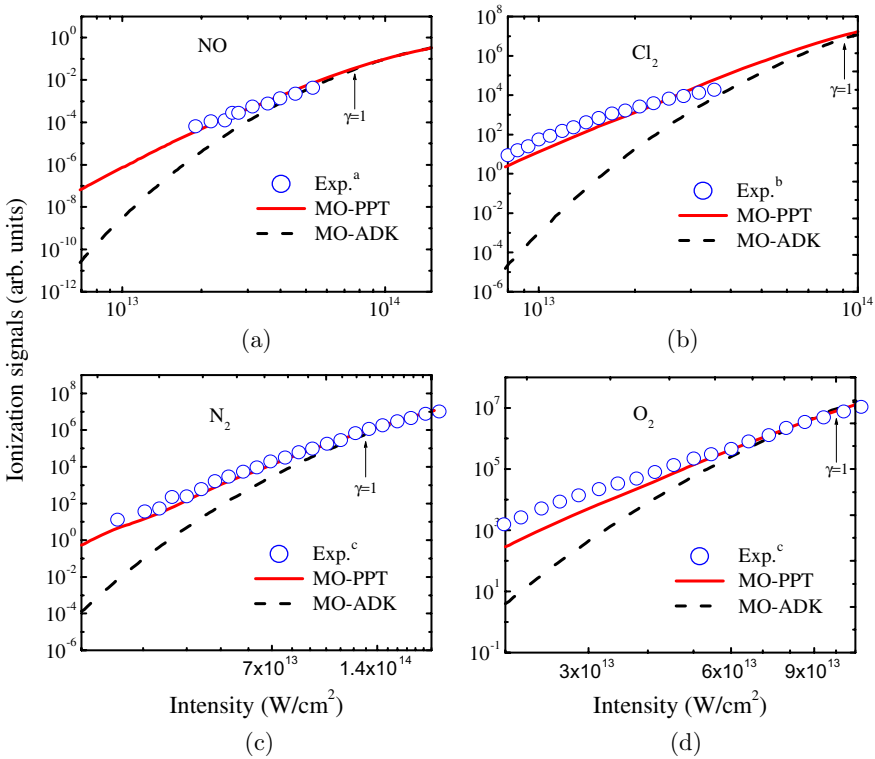

Fig. 10. (Color online) Ionization signals as a function of laser peak intensity. (a) NO at laser central wavelength $\lambda = 800\,\text{nm}$ and pulse duration (FWHM) $\tau = 25\,\text{fs}$; (b) Cl_2 at $\lambda = 790\,\text{nm}$ and $\tau = 25\,\text{fs}$; (c) N_2 at $\lambda = 800\,\text{nm}$ and $\tau = 30\,\text{fs}$; and (d) O_2 at $\lambda = 800\,\text{nm}$ and $\tau = 30\,\text{fs}$. The laser field is a Gaussian pulse in the calculations. Exp.[a] from Ref. [52], Exp.[b] from Ref. [61] and Exp.[c] from Ref. [124]. Adapted from [63]. © (2014) by Elsevier.

of HHG yields is determined mostly by the orbital symmetry within the molecular Lewenstein model. For example, the HOMO of N_2 (O_2) is a σ_g (π_g) orbital, thus both the HHG yields and electron density have a peak near $\theta = 0°$ ($\theta = 45°$) (see Figs. 11(a) and 11(b)). For the planar H_2O molecule, the alignment dependence of the 37th harmonic follows closely the angular distribution of electron density (see Figs. 11(c) and 11(d)). A Gaussian pulse with the laser intensity of $0.6 \times 10^{14}\,\text{W/cm}^2$, central wavelength of 1200 nm, and pulse duration of 25 fs was used in the calculation for H_2O. Therefore, the alignment-dependent HHG yields can be used to probe the molecular orbital from which the electron is removed if the contributions from other occupied orbitals to the HHG can be ignored. Note that these results are not surprising since in the molecular Lewenstein model only the initial wavefunction of the molecule enters into the theory. The original tomographic paper [9] was also based on the molecular Lewenstein model.

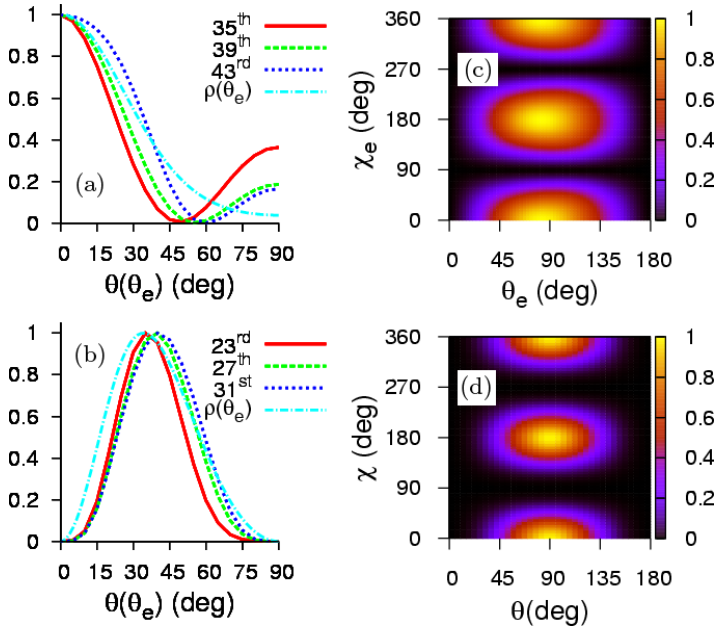

Fig. 11. (Color online) Comparison of alignment dependence of selected high-order harmonic yields in the plateau region and angular distribution of the asymptotic electron density for (a) N_2 and (b) O_2. (c) Angular distribution of electron density for the H_2O molecule; (d) Alignment dependence of the 37th harmonic from H_2O. For the laser parameters used, see text.

More accurate treatment of HHG like the QRS model [3, 103, 125] requires that the recombining electrons be described by scattering wavefunctions instead of plane waves used in the Lewenstein model. In addition, experimental HHG spectra are due to the coherent emission of light from all molecules in the medium and thus propagation effects should be included [126]. For HHG due to simpler molecules, such as N_2, O_2 and CO_2, accurate calculations based on the QRS model, including multiple orbital contributions as well as propagation effect, has been carried out and the results have been compared well with experiments [121, 127–129]. In fact, HHG from large polyatomic molecules have also been carried out within the QRS model [130–132]. Such calculations are quite tedious. In such situations, molecular Lewenstein model would offer a convenient qualitative theory for interpreting experimental observations.

4. Conclusions

In this chapter, it is shown that molecular orbital in a molecule can be directly probed using the alignment-dependent ionization probabilities or HHG yields from molecules exposed to an intense laser field. The ionization probabilities can be

calculated easily with simple models like MO-ADK, MO-PPT, MO-SFA *et al.* In the MO-ADK model, the static ionization rate depends on the structure parameters (i.e., expansion coefficients) of molecules. An efficient method to obtain the molecular wavefunction with the correct asymptotic behavior by solving the time-independent Schrödinger equation with the B-spline functions has been described where the one-electron potential is constructed numerically based on the DFT. These correct wavefunctions are used to extract accurate structure parameters of molecules in the asymptotic region. The failure of the MO-ADK model in the multiphoton regime was also addressed. Interestingly the MO-PPT model was able to fit both the TDSE results and the available experimental data covering from the multiphoton to tunneling ionization regimes. Based on the MO-ADK model, it is shown that tunneling ionization rates of inner orbitals are comparable to that of the HOMO at some alignment angles. Indeed, contributions from inner orbitals to strong-field phenomena have been observed experimentally [23, 27, 28, 31, 113–119]. Moreover, it is also demonstrated that the molecular orbital from which the electron is removed can be probed using alignment-dependent ionization probabilities or HHG signals by an intense laser field when the contributions from inner occupied orbitals can be neglected.

Acknowledgments

The authors thank Prof. X. M. Tong, Prof. T. F. Jiang, Prof. Zengxiu Zhao, Dr. Anh-Thu Le, Dr. Cheng Jin and Dr. Junliang Xu for their contributions on these researches. S. -F. Z would like to thank Dr. Shi-Lin Hu for providing their ionization probabilities obtained from the SAE-TDSE for H_2. CDL was supported in part by Chemical Sciences, Geosciences and Biosciences Division, Office of Basic Energy Sciences, Office of Science, U.S. Department of Energy. S. -F. Z and X. X. Z was also supported by the National Natural Science Foundation of China under Grant Nos. 11044007, 11164025, 11264036, 11465016 and the Specialized Research Fund for the Doctoral Program of Higher Education of China under Grant Nos. 20096203120001, and 20116203120001.

References

1. W. H. E. Schwarz, *Angew. Chem. Int. Ed.* 45, 1508 (2006).
2. A. D. Bandrauk and M. Ivanov (eds.), *Quantum Dynamic Imaging* (New York: Springer, 2011).
3. C. D. Lin, A. -T. Le, Z. Chen, T. Morishita, and R. R. Lucchese, *J. Phys. B: At. Mol. Opt. Phys.* **43**, 122001 (2010).
4. M. Lein, *J. Phys. B: At. Mol. Opt. Phys.* **40**, R135 (2007).
5. S. Haessler, J. Caillat, and P. Salières, *J. Phys. B: At. Mol. Opt. Phys.* **44**, 203001 (2011).
6. J. Repp and G. Meyer, *Phys. Rev. Lett.* **94**, 026803 (2005).
7. A. Bellec, F. Ample, D. Riedel, G. Dujardin, and C. Joachim, *Nano Lett.* **9**, 144 (2009).

8. P. Puschnig, S. Berkebile, A. J. Fleming, G. Koller, K. Emtsev, T. Seyller, J. D. Riley, C. Ambrosch-Draxl, F. P. Netzer, and M. G. Ramsey, *Science* **326**, 702 (2009).
9. J. Itatani, J. Levesque, D. Zeidler, H. Niikura, H. Pépin, J. C. Kieffer, P. B. Corkum, and D. M. Villeneuve, *Nature* (London) **432**, 867 (2004).
10. V. -H. Le, A. -T. Le, R. H. Xie, and C. D. Lin, *Phys. Rev. A* **76**, 013414 (2007).
11. C. Vozzi, M. Negro, F. Calegari, G. Sansone, M. Nisoli, S. De Silvestri, and S. Stagira, *Nat. Phys.* **7**, 822 (2011).
12. Y. Li, X. Zhu, P. Lan, Q. Zhang, M. Qin, and P. Lu, *Phys. Rev. A* **89**, 045401 (2014).
13. S. Patchkovskii, Z. X. Zhao, T. Brabec, and D. B. Villeneuve, *Phys. Rev. Lett.* **97**, 123003 (2006).
14. Y. J. Chen, L. B. Fu, and J. Liu, *Phys. Rev. Lett.* **111**, 073902 (2013).
15. P. B. Corkum, *Phys. Rev. Lett.* **71**, 1994 (1993).
16. I. V. Litvinyuk, K. F. Lee, P. W. Dooley, D. M. Rayner, D. M. Villeneuve, and P. B. Corkum, *Phys. Rev. Lett.* **90**, 233003 (2003).
17. D. Pavičić, K. F. Lee, D. M. Rayner, P. B. Corkum, and D. M. Villeneuve, *Phys. Rev. Lett.* **98**, 243001 (2007).
18. I. Thomann, R. Lock, V. Sharma, E. Gagnon, S. T. Pratt, H. C. Kapteyn, M. M. Murnane, and W. Li, *J. Phys. Chem. A* **112**, 9382 (2008).
19. V. Kumarappan, L. Holmegaard, C. Martiny, C. B. Madsen, T. K. Kjeldsen, S. S. Viftrup, L. B. Madsen, and H. Stapelfeldt, *Phys. Rev. Lett.* **100**, 093006 (2008).
20. R. Itakura, H. Hasegawa, Y. Kurosaki, A. Yokoyama, and Y. Ohshima, J. *Phys. Chem. A* **114**, 11202 (2010).
21. J. L. Hansen, L. Holmegaard, J. H. Nielsen, H. Stapelfeldt, D. Dimitrovski, and L. B. Madsen, *J. Phys. B: At. Mol. Opt. Phys.* **45**, 015101 (2012).
22. A. Staudte, S. Patchkovskii, D. Pavičić, H. Akagi, O. Smirnova, D. Zeidler, M. Meckel, D. M. Villeneuve, R. Dörner, M. Yu. Ivanov, and P. B. Corkum, *Phys. Rev. Lett.* **102**, 033004 (2009).
23. H. Akagi, T. Otobe, A. Staudte, A. Shiner, F. Turner, R. Dörner, D. M. Villeneuve, and P. B. Corkum, *Science* **325**, 1364 (2009).
24. M. Magrakvelidze, F. He, S. De, I. Bocharova, D. Ray, U. Thumm, and I. V. Litvinyuk, *Phys. Rev. A* **79**, 033408 (2009).
25. J. Wu, M. Meckel, S. Voss, H. Sann, M. Kunitski, L. Ph. H. Schmidt, A. Czasch, H. Kim, T. Jahnke, and R. Dörner, *Phys. Rev. Lett.* **108**, 043002 (2012).
26. J. B. Williams, C. S. Trevisan, M. S. Schöffler, T. Jahnke, I. Bocharova, H. Kim, B. Ulrich, R. Wallauer, F. Sturm,T. N. Rescigno, A. Belkacem, R. Dörner, Th. Weber, C. W. McCurdy, and A. L. Landers, *Phys. Rev. Lett.* **108**, 233002 (2012).
27. J. Wu, L. Ph. H. Schmidt, M. Kunitski, M. Meckel, S. Voss, H. Sann, H. Kim, T. Jahnke, A. Czasch, and R. Dörner, *Phys. Rev. Lett.* **108**, 183001 (2012).
28. H. Liu, S. -F. Zhao, M. Li, Y. Deng, C. Wu, X. X. Zhou, Q. Gong, and Y. Liu, *Phys. Rev. A* **88**, 061401 (R) (2013).
29. A. S. Alnaser, S. Voss, X. M. Tong, C. M. Maharjan, P. Ranitovic, B. Ulrich, T. Osipov, B. Shan, Z. Chang, and C. L. Cocke, *Phys. Rev. Lett.* **93**, 113003 (2004).
30. A. S. Alnaser, C. M. Maharjan, X. M. Tong, B. Ulrich, P. Ranitovic, B. Shan, Z. Chang, C. D. Lin, C. L. Cocke, and I. V. Litvinyuk, *Phys. Rev. A* **71**, 031403(R) (2005).
31. P. von den Hoff, I. Znakovskaya, S. Zherebtsov, M. F. Kling, and R. de Vivie-Riedle, *Appl. Phys. B* **98**, 659 (2010).
32. X. Liu, C. Wu, Z. Wu, Y. Liu, Y. Deng, and Q. Gong, *Phys. Rev. A* **83**, 035403 (2011).
33. H. Chen, L. Fang, V. Tagliamonti, and G. N. Gibson, *Phys. Rev. A* **84**, 043427 (2011).
34. J. McKenna, A. M. Sayler, B. Gaire, Nora G. Johnson, K. D. Carnes, B. D. Esry, and I. Ben-Itzhak, *Phys. Rev. Lett.* **103**, 103004 (2009).
35. S. Petretti, Y. V. Vanne, A. Saenz, A. Castro, and P. Decleva, *Phys. Rev. Lett.* **104**, 223001 (2010).

36. M. Spanner and S. Patchkovskii, *Phys. Rev. A* **80**, 063411 (2009).
37. T. K. Kjeldsen, L. A. A. Nikolopoulos, and L. B. Madsen, *Phys. Rev. A* **75**, 063427 (2007).
38. M. Abu-samha and L. B. Madsen, *Phys. Rev. A* **80**, 023401 (2009).
39. M. Abu-samha and L. B. Madsen, *Phys. Rev. A* **81**, 033416 (2010).
40. G. Lagmago Kamta and A. D. Bandrauk, *Phys. Rev. A* **74**, 033415 (2006).
41. Y. J. Jin, X. M. Tong, and N. Toshima, *Phys. Rev. A* **83**, 063409 (2011).
42. B. Zhang, J. Yuan, and Z. X. Zhao, *Phys. Rev. A* **85**, 033421 (2012).
43. M. Awasthi, Y. V. Vanne, A. Saenz, A. Castro, and P. Decleva, *Phys. Rev. A* **77**, 063403 (2008).
44. S. Petretti , A. Saenz, A. Castro, and P. Decleva, *Chem. Phys.* **414**, 45 (2013).
45. S. K. Son and Shih-I. Chu, *Phys. Rev. A* **80**, 011403(R) (2009).
46. D. A. Telnov and Shih-I. Chu, *Phys. Rev. A* **79**, 041401(R) (2009).
47. X. Chu, *Phys. Rev. A* **82**, 023407 (2010).
48. X. Chu and M. McIntyre, *Phys. Rev. A* **83**, 013409 (2011).
49. T. Otobe and K. Yabana, *Phys. Rev. A* **75**, 062507 (2007).
50. S. K. Son and Shih-I Chu, *Chem. Phys.* **366**, 91 (2009).
51. B. Zhang, J. Yuan, and Z. X. Zhao, *Phys. Rev. Lett.* **111**, 163001 (2013).
52. X. M. Tong, Z. X. Zhao, and C. D. Lin, *Phys. Rev. A* **66**, 033402 (2002).
53. Z. X. Zhao, X. M. Tong, and C. D. Lin, *Phys. Rev. A* **67**, 043404 (2003).
54. S. -F. Zhao, C. Jin, A. -T. Le, T. F. Jiang, and C. D. Lin, *Phys. Rev. A* **81**, 033423 (2010).
55. S. -F. Zhao, J. Xu, C. Jin, A. -T. Le, and C. D. Lin, *J. Phys. B: At. Mol. Opt. Phys.* **44**, 035601 (2011).
56. J. Muth-Böhm, A. Becker, and F. H. M. Faisal, *Phys. Rev. Lett.* **85**, 2280 (2000).
57. T. K. Kjeldsen and L. B. Madsen, *J. Phys. B: At. Mol. Opt. Phys.* **37**, 2033 (2004).
58. D. B. Milošević, *Phys. Rev. A* **74**, 063404 (2006).
59. B. Zhang and Z. X. Zhao, *Phys. Rev. A* **82**, 035401 (2010).
60. Y. J. Chen and B. Zhang, *J. Phys. B: At. Mol. Opt. Phys.* **45**, 215601 (2012).
61. E. P. Benis, J. F. Xia, X. M. Tong, M. Faheem, M. Zamkov, B. Shan, P. Richard, and Z. Chang, *Phys. Rev. A* **70**, 025401 (2004).
62. Y. Z. Fu, S. -F. Zhao, and X. X. Zhou, *Chin. Phys. B* **21**, 113101 (2012).
63. S. -F. Zhao, L. Liu, and X. X. Zhou, *Opt. Commun.* **313**, 74 (2014).
64. L. B. Madsen, O. I. Tolstikhin, and T. Morishita, *Phys. Rev. A* **85**, 053404 (2012).
65. L. B. Madsen, F. Jensen, O. I. Tolstikhin, and T. Morishita, *Phys. Rev. A* **87**, 013406 (2013).
66. L. B. Madsen, F. Jensen, O. I. Tolstikhin, and T. Morishita, *Phys. Rev. A* **89**, 033412 (2014).
67. R. Murray, M. Spanner, S. Patchkovskii, and M. Yu. Ivanov, *Phys. Rev. Lett.* **106**, 173001 (2011).
68. G. A. Gallup and I. I. Fabrikant, *Phys. Rev. A* **81**, 033417 (2010).
69. B. Zhang and Z. X. Zhao, *Chin. Phys. Lett.* **27**, 043301 (2010).
70. M. V. Ammosov, N. B. Delone, and V. P. Krainov, Zh. Eksp. Teor. Fiz. 91, 2008 (1986) [(*Sov. Phys. JETP* **64**, 1191 (1986)].
71. D. Dill and J. L. Dehmer, *J. Chem. Phys.* **61**, 692 (1974).
72. M. J. Frisch, G. W. Trucks, H. B. Schlegel, G. E. Scuseria, M. A. Robb, J. R. Cheeseman, J. A. Montgomery Jr., T. Vreven, K. N. Kudin, J. C. Burant, J. M. Millam, S. S. Iyengar, J. Tomasi, V. Barone, B. Mennucci, M. Cossi, G. Scalmani, N. Rega, G. A. Petersson, H. Nakatsuji, M. Hada, M. Ehara, K. Toyota, R. Fukuda, J. Hasegawa, M. Ishida, T. Nakajima, Y. Honda, O. Kitao, H. Nakai, M. Klene, X. Li, J. E. Knox, H. P. Hratchian, J. B. Cross, V. Bakken, C. Adamo, J. Jaramillo, R. Gomperts, R. E. Stratmann, O. Yazyev, A. J. Austin, R. Cammi, C. Pomelli, J. W. Ochterski, P. Y. Ayala, K. Morokuma, G. A. Voth, P. Salvador, J. J. Dannenberg,V. G. Zakrzewski, S. Dapprich, A. D. Daniels, M. C. Strain, O. Farkas, D. K. Malick, A. D. Rabuck, K. Raghavachari, J. B. Foresman, J. V. Ortiz, Q. Cui, A. G. Baboul, S. Clifford, J. Cioslowski, B. B. Stefanov, G. Liu, A. Liashenko, P. Piskorz, I. Komaromi, R. L. Martin, D. J. Fox, T. Keith, M. A. Al-Laham, C. Y. Peng, A. Nanayakkara, M. Challacombe,

P. M. W. Gill, B. Johnson, W. Chen, M. W. Wong, C. Gonzalez, and J. A. Pople, GAUSSIAN 03, Revision C.02 (Gaussian Inc. Pittsburgh, PA, 2003).
73. M. W. Schmidt, K. K. Baldridge, J. A. Boatz, S. T. Elbert, M. S. Gordon, J. H. Jensen, S. Koseki, N. Matsunaga, K. A. Nguyen, S. Su, T. L. Windus, M. Dupuis, and J. A. Montgomery Jr., *J. Comput. Chem.* **14**, 1347 (1993).
74. H. -J. Werner and P. J. Knowles, MOLPRO, Version 2002.6, A Package of Ab Initio Programs, Birmingham, UK, 2003.
75. J. Kobus, L. Laaksonen, and D. Sundholm, *Comput. Phys. Commun.* **98**, 346 (1996).
76. A. -T. Le, X. M. Tong, and C. D. Lin, *J. Mod. Opt.* **54**, 967 (2007).
77. T. K. Kjeldsen, C. Z. Bisgaard, L. B. Madsen, and H. Stapelfeldt, *Phys. Rev. A* **71**, 013418 (2005).
78. S. -F. Zhao, C. Jin, A. -T. Le, T. F. Jiang, and C. D. Lin, *Phys. Rev. A* **80**, 051402 (R) (2009).
79. S. -F. Zhao, C. Jin, A. -T. Le, and C. D. Lin, *Phys. Rev. A* **82**, 035402 (2010).
80. J. P. Wang, S. -F. Zhao, C. R. Zhang, W. Li, and X. X. Zhou, *Mol. Phys.* **112**, 1102 (2014).
81. X. J. Li, S. -F. Zhao, and X. X. Zhou, *Commun. Theor. Phys.* **58**, 419 (2012).
82. T. K. Kjeldsen and L. B. Madsen, *Phys. Rev. A* **71**, 023411 (2005).
83. R. Torres, N. Kajumba, Jonathan G. Underwood, J. S. Robinson, S. Baker, J. W. G. Tisch, R. de Nalda,W. A. Bryan, R. Velotta, C. Altucci, I. C. E. Turcu, and J. P. Marangos, *Phys. Rev. Lett.* **98**, 203007 (2007).
84. M. Lein, N. Hay, R. Velotta, J. P. Marangos, and P. L. Knight, *Phys. Rev. Lett.* **88**, 183903 (2002).
85. G. Lagmago Kamta and A. D. Bandrauk, *Phys. Rev. A* **71**, 053407 (2005).
86. G. Lagmago Kamta and A. D. Bandrauk, *Phys. Rev. A* **80**, 041403 (R) (2009).
87. D. A. Telnov and Shih-I Chu, *Phys. Rev. A* **76**, 043412 (2007).
88. X. B. Bian and A. D. Bandrauk, *Phys. Rev. Lett.* **105**, 093903 (2010).
89. X. B. Bian and A. D. Bandrauk, *Phys. Rev. A* **86**, 053417 (2012).
90. D. A. Telnov and Shih-I Chu, *Phys. Rev. A* **80**, 043412 (2009).
91. X. Chu and G. C. Groenenboom, *Phys. Rev. A* **87**, 013434 (2013).
92. E. P. Fowe and A. D. Bandrauk, *Phys. Rev. A* **84**, 035402 (2011).
93. E. F. Penka, E. Couture-Bienvenue, and A. D. Bandrauk, *Phys. Rev. A* **89**, 023414 (2014).
94. X. X. Zhou, X. M. Tong, Z. X. Zhao, and C. D. Lin, *Phys. Rev. A* **71**, 061801 (R) (2005).
95. X. X. Zhou, X. M. Tong, Z. X. Zhao, and C. D. Lin, *Phys. Rev. A* **72**, 033412 (2005).
96. A. -T. Le, X. M. Tong, and C. D. Lin, *Phys. Rev. A* **73**, 041402 (R) (2006).
97. J. P. Marangos, C. Altucci, R. Velotta, E. Heesel, E. Springate, M. Pascolini, L. Poletto, P. Villoresi, C. Vozzi, G. Sansone, M. Anscombe, J.-P. Caumes, S. Stagira, and M. Nisoli, *J. Mod. Opt.* **53**, 97 (2006).
98. S. Odžak and D. B. Milošević, *Phys. Rev. A* **79**, 023414 (2009).
99. C. B. Madsen and L. B. Madsen, *Phys. Rev. A* **74**, 023403 (2006).
100. C. B. Madsen and L. B. Madsen, *Phys. Rev. A* 76, 043419 (2007).
101. Y. J. Chen and B. Hu, *Phys. Rev. A* 80, 033408 (2009).
102. M. Lewenstein, Ph. Balcou, M. Yu. Ivanov, A. L'Huillier, and P. B. Corkum, *Phys. Rev. A* 49, 2117 (1994).
103. A. -T. Le, R. R. Lucchese, S. Tonzani, T. Morishita, and C. D. Lin, *Phys. Rev. A* 80, 013401 (2009).
104. P. R. T. Schipper, O. V. Gritsenko, S. J. A. van Gisbergen, and E. J. Baerends, *J. Chem. Phys.* **112**, 1344 (2000).
105. Shih-I Chu, *J. Chem. Phys.* **123**, 062207 (2005).
106. J. P. Perdew and Y. Wang, *Phys. Rev. B* **45**, 13244 (1992).
107. X. B. Bian, L. Y. Peng, and T. Y. Shi, *Phys. Rev. A* **77**, 063415 (2008).
108. A. M. Perelomov, V. S. Popov, and M. V. Terent'ev, *Sov. Phys. JETP* **23**, 924 (1966).
109. F. A. Ilkov, J. E. Decker, and S. L. Chin, J. *Phys. B: At. Mol. Opt. Phys.* **25**, 4005 (1992).
110. S. -F. Zhao, C. Jin, R. R. Lucchese, A. -T. Le, and C. D. Lin, *Phys. Rev. A* **83**, 033409 (2011).

111. Y. -M. Lee, T. -F. Jiang, Z. -Y. Su, and J. -S. Wu, *Comput. Phys. Commun.* **182**, 140 (2011).
112. S. L. Hu, Z. X. Zhao, and T. Y. Shi, *Chin. Phys. Lett.* **30**, 103103 (2013).
113. C. Wu, H. Zhang, H. Yang, Q. Gong, D. Song, and H. Su, *Phys. Rev. A* **83**, 033410 (2011).
114. I. Znakovskaya, P. Von den Hoff, S. Zherebtsov, A. Wirth, O. Herrwerth, M. J. J. Vrakking, R. de Vivie-Riedle, and M. F. Kling, *Phys. Rev. Lett.* **103**, 103002 (2009).
115. B. K. McFarland, J. P. Farrell, P. H. Bucksbaum, and M. Gühr, *Science* **322**, 1232 (2008).
116. O. Smirnova, Y. Mairesse, S. Patchkovskii, N. Dudovich, D. Villeneuve, P. B. Corkum, and M. Yu. Ivanov, *Nature* (London) **460**, 972 (2009).
117. H. J. Wörner, J. B. Bertrand, P. Hockett, P. B. Corkum, and D. M. Villeneuve, *Phys. Rev. Lett.* **104**, 233904 (2010).
118. Z. Diveki, A. Camper, S. Haessler, T. Auguste, T. Ruchon, B. Carré, P. Salières, R. Guichard, J. Caillat, A. Maquet, and R. Taïeb, *New J. Phys.* **14**, 023062 (2012).
119. J. Li, P. Liu, H. Yang, L. Song, S. Zhao, H. Lu, R. Li, and Z. Xu, *Opt. Express* **21**, 7599 (2013).
120. A. -T. Le, R. R. Lucchese, and C. D. Lin, *J. Phys. B: At. Mol. Opt. Phys.* **42**, 211001 (2009).
121. C. Jin, J. B. Bertrand, R. R. Lucchese, H. J. Wörner, P. B. Corkum, D. M. Villeneuve, A. -T. Le, and C. D. Lin, *Phys. Rev. A* **85**, 013405 (2012).
122. J. Heslar, D. Telnov, and Shih-I Chu, *Phys. Rev. A* **83**, 043414 (2011).
123. X. M. Tong and C. D. Lin, *J. Phys. B: At. Mol. Opt. Phys.* **38**, 2593 (2005).
124. C. Guo, M. Li, J. P. Nibarger, and G. N. Gibson, *Phys. Rev. A* **58**, R4271 (1998).
125. T. Morishita, A. -T. Le, Z. Chen, and C. D. Lin, *Phys. Rev. Lett.* **100**, 013903 (2008).
126. C. Jin, A. -T. Le, and C. D. Lin, *Phys. Rev. A* **79**, 053413 (2009).
127. C. Jin, A. -T. Le, and C. D. Lin, *Phys. Rev. A* **83**, 023411 (2011).
128. C. Jin, H. J. Wörner, V. Tosa, A. -T. Le, J. B. Bertrand, R. R. Lucchese, P. B. Corkum, D. M. Villeneuve, and C. D. Lin, *J. Phys. B: At. Mol. Opt. Phys.* **44**, 095601 (2011).
129. C. Jin, A. -T. Le, and C. D. Lin, *Phys. Rev. A* **83**, 053409 (2011).
130. A. -T. Le, R. R. Lucchese, M. T. Lee, and C. D. Lin, *Phys. Rev. Lett.* **102**, 203001 (2009).
131. M. C. H. Wong, A. -T. Le, A. F. Alharbi, A. E. Boguslavskiy, R. R. Lucchese, J. -P. Brichta, C. D. Lin, and V. R. Bhardwaj, *Phys. Rev. Lett.* **110**, 033006 (2013).
132. A. -T. Le, R. R. Lucchese, and C. D. Lin, *Phys. Rev. A* **88**, 021402 (R) (2013).